Flash Heat Treatment Constructing Organic-Inorganic Hybrid Layer for High-Performance Silicon Anode

Haoyu Hu [1], Tonghui Cai [2], Junbin Wang [1], Jixian Cao [1], Wei Xing [1, *]

[1] School of Materials Science and Engineering, State Key Laboratory of Heavy Oil Processing, China University of Petroleum (East China), Qingdao 266580, P.R. China.

[2] School of New Energy, Nanjing University of Science & Technology, Nanjing 210094, P.R. China.

* Corresponding Author Email: xingwei@upc.edu.cn

Abstract. The commercialization of silicon (Si) anodes has long faced critical challenges of severe volume expansion and poor conductivity. While traditional surface coating strategies can mitigate these issues, rigid carbon coatings exhibit poor stress tolerance, and flexible organic polymers with polymer networks lack sufficient electron/ion conductivity. This study developed a novel flash heat treatment strategy. By subjecting polypyrrole (PPy)-coated nano-silicon (nmSi) to short-duration high-temperature treatment, we achieved partial carbonization of the PPy shell, resulting in a core-shell silicon material (nmSi@PCHS) featuring a unique organic polymer/inorganic carbon (PPy/C) hybrid layer. After optimizing treatment time, nmSi@PCHS-5 demonstrated optimal electrochemical performance: exceptional long-term cycling stability (1000 mAh/g after 500 cycles) and superior rate capability (1200 mAh/g at 5 A/g). The performance enhancement stems from the synergistic effect of the C/PPy hybrid shell: the carbon component significantly improves electrical conductivity and lithium-ion transport, while the retained PPy network provides inherent elasticity and toughness, effectively buffering silicon volume changes and maintaining structural integrity during cycling. This work demonstrates that flash heat treatment can create multifunctional hybrid interfacial layers that effectively optimize conductivity and mechanical resilience in synergy, offering unique insights for developing high-performance silicon-based anodes.

Keywords: Lithium-ion batteries, silicon anode, organic-inorganic hybrid layer.

1. Introduction

The theoretical capacity limit of traditional graphite anodes (372 mAh/g) can no longer meet the ever-increasing demands for lithium-ion battery performance in end applications, making it imperative to accelerate the commercialization of high-energy-density lithium-ion batteries (LIBs, targeting 500 Wh/kg).[1, 2] Silicon (Si) anodes are widely regarded as the most promising high-capacity anode material for next-generation LIBs due to their exceptional theoretical capacity (up to 3590 mAh/g at room temperature), abundant raw material sources, low discharge potential (~370 mV vs. Li/Li^+), and environmental friendliness.[3, 4] However, significant volume changes during cycling cause structural damage and excessive growth of the solid electrolyte interphase (SEI), leading to severe side reactions and electrode deactivation. These issues compromise battery cycle life and coulombic efficiency, thereby hindering commercial adoption.[5-8]

Surface functionalization modification serves as an effective strategy to address these challenges: By forming a nanoscale coating layer, it isolates direct contact between silicon materials and the electrolyte, significantly reducing side reactions and irreversible capacity loss while mitigating volume variations, thereby markedly enhancing the lithium-ion storage performance of silicon anodes.[9] Currently, coating materials for silicon anode surface modification are primarily categorized into inorganic and organic types. Inorganic materials mainly include carbon, metal oxides, and silicon oxides, while organic materials mainly encompass polymers such as polyaniline (PANI) and polyacrylonitrile (PAN).[10-14] Different materials typically possess distinct properties, such as mechanical strength, electrical conductivity, electrochemical stability, and ion permeability. Among them, carbon-based coatings are preferred due to their wide availability of raw materials, simple synthesis, good electrical conductivity, and chemical stability. However, rigid carbon coatings are

prone to fracture under accumulated stress during long-term cycling, leading to silicon surface exposure and severe side reactions. Additionally, the weak interfacial bonding between carbon and silicon often results in sluggish electrode kinetics and structural instability. In contrast, organic polymers exhibit superior adaptability to volume changes due to the inherent elasticity of their macromolecular networks. For instance, Zheng et al. prepared a silicon capsule material Si@PMMA with a poly (methyl methacrylate) (PMMA) shell via in-situ microemulsion polymerization.[11] This approach preserved the intrinsic activity of silicon particles while leveraging PMMA's high elasticity, viscosity in electrolytes, and stability. Simultaneously, the PMMA shell enhances the lithium-ion diffusion coefficient (DLi^+) in silicon anodes, facilitating the formation of a stable and flexible solid-electrolyte interphase (SEI) on the silicon surface, significantly improving the cycling and rate performance of silicon particles. Therefore, designing a functionalized coating combining inorganic carbon with organic polymers holds significant value for silicon anodes experiencing large volume expansion. However, the design of carbon coatings on silicon anodes typically requires high-temperature treatment, under which most organic polymers would pyrolyze and lose their original properties, making it challenging to achieve coexistence with carbon coatings.

In summary, to establish effective coatings on the silicon nanoparticle surface for enhanced performance, the coating must meet the following requirements: 1) sufficient mechanical strength to buffer the volume changes of the silicon core; 2) excellent electronic and ionic conductivity;[15] 3) strong bonding with the silicon core to compensate for silicon's slow kinetic characteristics; 4) electrochemical stability in the electrolyte; 5) appropriate flexibility to withstand repeated stress impacts. However, no single coating material can simultaneously fulfill all these requirements. Therefore, designing a silicon anode coating with ideal mechanical properties (balancing strength and toughness) and sufficient electronic/ionic conductivity is crucial for advancing industrial applications of silicon anodes, while also being highly challenging.[16]

In this study, we developed a flash heat treatment method wherein pretreated samples were directly placed into a preheated tube furnace at high temperature. Following short-duration (on the order of minutes) heat treatment, the samples were rapidly withdrawn, causing partial carbonization of the surface-pretreated PPy coating and forming a PPy/C hybrid phase shell. The nmSi@PCHS material prepared via this method exhibited significantly enhanced stability and rate capability, maintaining a capacity exceeding 1000 mAh/g after 500 long cycles. Subsequent systematic investigations using X-ray diffraction (XRD), Raman spectroscopy, and scanning electron microscopy (SEM) characterized the composite material's properties, while detailed electrochemical analyses elucidated the root causes of this performance enhancement.

2. Experiment section

2.1. Reagents and apparatus

Nano-silicon (nmSi) particles (~100nm) were purchased from Ningbo Jinlei Nano Materials Technology Co., Ltd., pyrrole was purchased from Aladdin Chemical Reagent Co., Ltd., and sodium dodecyl sulfate (SDS), anhydrous ethanol, ammonium persulfate ($(NH_4)_2S_2O_8$), and hydrochloric acid (HCl) were all purchased from Sinopharm Chemical Reagent Co., Ltd. All reagents were of analytical grade purity and were used directly without purification. The water used in the experiments was deionized water prepared in the laboratory. The heat treatment equipment was a tube furnace that was self-designed and modified.

The physical phases of the materials were characterized using X-ray diffraction (XRD, Shimadzu XRD-7000) and Raman spectroscopy (HORIBA HR Evolution). Obtain the thermogravimetric curves of the materials through a synchronous thermal analyzer (Discovery SDT). The microstructure of the materials and electrodes was examined in detail using high-resolution scanning electron microscopy (SEM, Hitachi Regulus8100) and field-emission scanning transmission electron microscopy (STEM, Thermo Fisher Talos F200X).

2.2. Sample preparation

Add nano-silicon (150mg) to an SDS solution (5mg), mix uniformly, and stir for 6 hours. Transfer the mixture to a sandwich beaker, then sequentially add pyrrole monomer (140 μL), HCl (1M, 0.5ml), and $(NH_4)_2S_2O_8$ (0.114g, 5ml). React under vigorous stirring at 0°C for 3h. Filter the resulting suspension through polyester fiber (Carpenter Co.), wash with deionized water until neutral, then transfer the product to a vacuum oven for overnight drying at 50°C. Subject the dried product to flash heat treatment at 800°C under N_2 atmosphere for 1min, 3min, 5min, and 7min respectively. For comparison, prepare control groups: nmSi@PPy (without heat treatment) and nmSi@C (heated at the same temperature for 2h). Designate the flash-treated samples as nmSi@PCHS-1, nmSi@PCHS-3, nmSi@PCHS-5, and nmSi@PCHS-7.

2.3. Fabrication of the electrochemical cell

Active material, conductive additive (Super P), and binder (Polyacrylic acid, PAA) were added at a mass ratio of 6:2:2. Using deionized water as the dispersant, the mixture was stirred overnight in a weighing bottle. Subsequently, the mixture was uniformly coated onto copper foil and vacuum-dried at 60°C for 12 hours. The coated foil was then cut into 12 mm diameter circular electrodes for use. Using lithium foil as the counter electrode, CR2032-type coin cells were assembled in an argon-filled glove box at room temperature. Celgard 2500 was selected as the separator, with 40-50 μL of commercial electrolyte (containing 5% FEC) added.

2.4. Electrochemical measurements

Constant-current charge-discharge tests (0.01-1.2 V vs. Li/Li^+) and rate performance tests (0.01-1.2 V vs. Li/Li^+) were conducted on a Land CT2001A system. Cyclic voltammetry (CV) (0.01-1.5 V vs. Li/Li^+) and electrochemical impedance spectroscopy (EIS) (0.01-105 Hz) measurements were performed using an electrochemical workstation (Bio-Logic SAS).

3. Results and Discussion

As shown in Figure 1, the nanosilicon (nmSi) raw material used is quasi-spherical with a diameter of approximately 150 nm (Fig. 1a and b). Subsequently, X-ray diffraction (XRD) and Raman spectroscopy revealed distinct characteristic peaks of crystalline Si (Fig. 1c and d). In XRD, sharp characteristic peaks at 28.4°, 47.3°, 56.1°, and 69.2° correspond to the (111), (220), (311), and (400) crystal planes, respectively, while the sharp peak near 520 cm^{-1} in the Raman spectrum indicates the first-order optical phonon vibration of the Si-Si bond. This demonstrates that the nanosilicon particles possess good long-range ordering and a highly crystalline nature. Comparing the XRD spectra of PPy and PPy-C, neither exhibits sharp crystalline characteristic peaks, indicating their amorphous nature. The broad peak in PPy-C confirms that it primarily exists as amorphous carbon after carbonization, making it difficult to distinguish the PPy phase from the carbon phase using XRD. Due to the richer chemical bonds and functional group vibrational modes (e.g., C-N, N-H) in PPy's polymer chains, it shows more characteristic peaks in Raman spectroscopy. After carbonization, PPy loses most heteroatoms, and its Raman spectrum displays the peak profile characteristic of disordered carbon. Therefore, we can utilize Raman spectroscopy to unambiguously confirm the presence of the PPy phase.

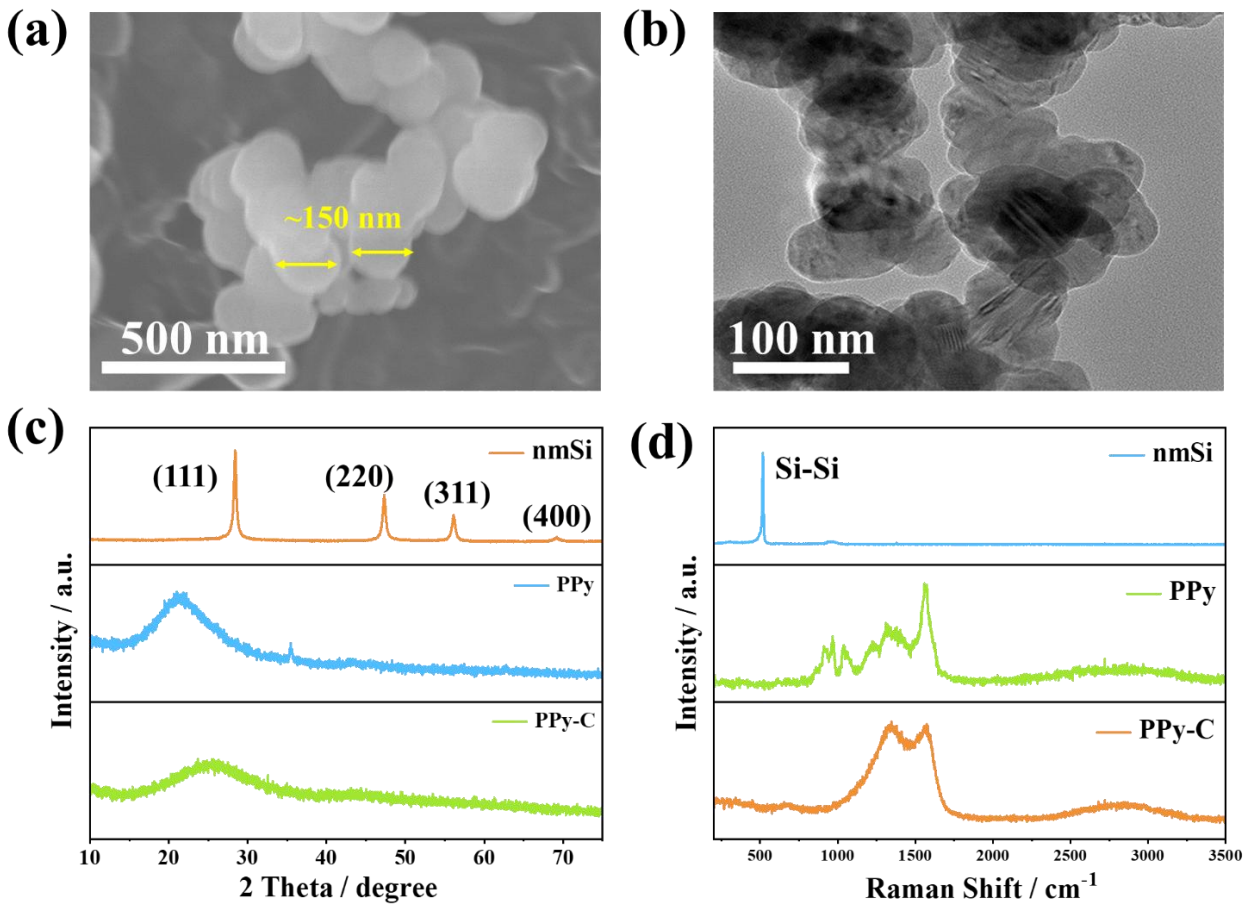

Fig 1. (a) SEM and (b) TEM images of nmSi.
(c) XRD and (d) Raman spectra of nmSi, PPy and PPy-C.

Subsequent constant current charge-discharge tests compared the cycling stability of relevant control groups. Initially, untreated nmSi electrodes exhibited poor cycling stability, with significant capacity fading within the first 100 cycles. In contrast, both nmSi@PPy and nmSi@C showed markedly improved stability. nmSi@C delivered higher initial capacity due to its highly carbonized surface shell providing excellent conductivity for capacity release; however, its subsequent cycle decay became pronounced due to the limited stress tolerance of the rigid carbon shell (Fig. 2a). Similarly, samples with different flash heat treatment durations displayed significantly divergent cycling stability (Fig. 2b). At 1min treatment, insufficient pyrolysis time prevented most PPy from converting to carbon structures, resulting in inadequate electronic/ionic conductivity and low capacity. At 3min and 5min treatments, capacity substantially increased while maintaining favorable cycling stability. Specifically, nmSi@PCHS-5 achieved optimal capacity and stability, indicating its ideal structure synergizing carbon's rigid conductive network with PPy's flexible polymeric skeleton. At 7min treatment, excessive PPy carbonization increased shell rigidity, causing stress accumulation and subsequent fracture during later cycles that rapidly degraded capacity. Furthermore, comparative analysis of cycling performance among nmSi@PCHS-5, nmSi, nmSi@PPy and nmSi@C confirmed the superior synergistic high-capacity and stability of nmSi@PCHS-5 (Fig. 2c-e). Simultaneously, its charge-discharge cycling and coulombic efficiency (CE) demonstrated stable operation with nearly 100% efficiency, verifying structural integrity, suppressed side reactions, and excellent reversibility (Fig. 2f). Finally, rate capability testing showed nmSi@PCHS-5 delivered approximately 2050 mAh/g at 1 A/g and maintained 1200 mAh/g even at 5 A/g. Capacity recovered to 2000 mAh/g when current density returned to 1 A/g, demonstrating exceptional rate performance (Fig. 3a).

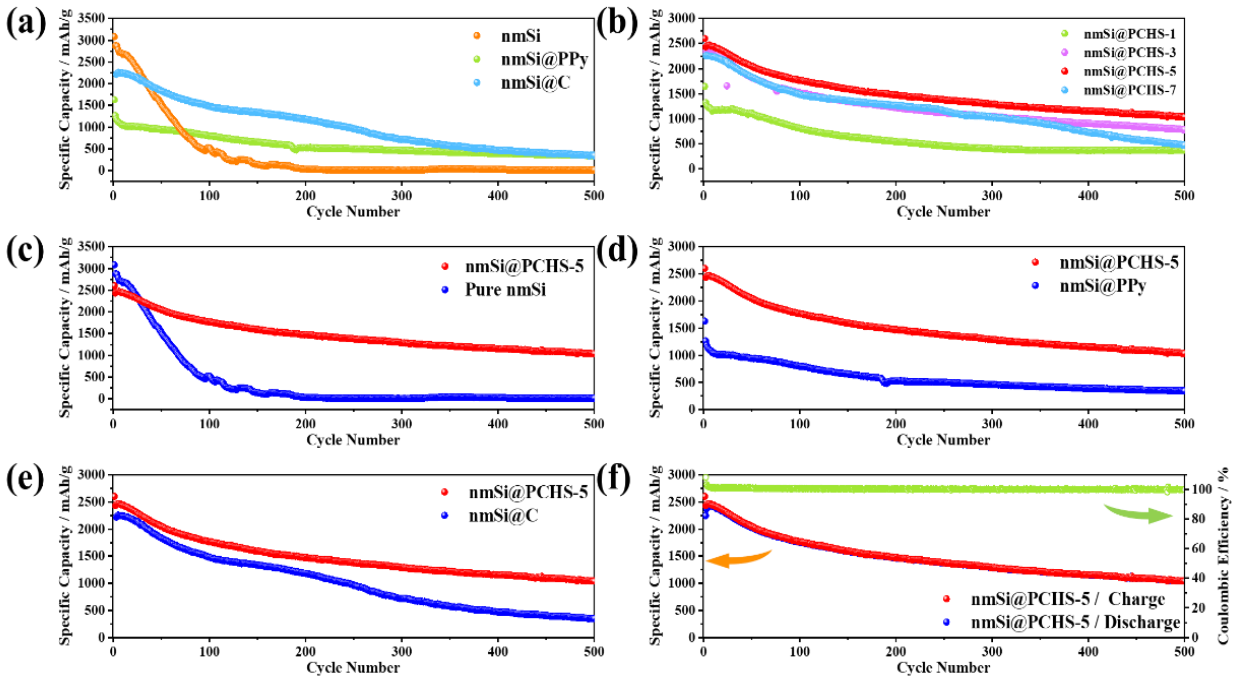

Fig 2. Reversible capacity performance at 1 A/g of (a) nmSi, nmSi@PPy and nmSi@C, (b) nmSi@PCHS with different processing times, (c) nmSi@PCHS-5 and Pure nmSi, (d) nmSi@PCHS-5 and nmSi@PPy, (e) nmSi@PCHS-5 and nmSi@C, (f) nmSi@PCHS-5 with coulombic efficiency.

XRD and Raman spectroscopy confirmed the crystalline structural characteristics of the composite materials, with nmSi@PCHS-1 excluded from further analysis due to insufficient processing time. All samples exhibited distinct characteristic peaks of crystalline silicon, indicating preserved crystallinity. The Raman spectra of nmSi@PCHS-3, nmSi@PCHS-5, and nmSi@PCHS-7 displayed not only peaks corresponding to Si-Si vibrations but also prominent characteristic peaks of PPy and C, confirming the formation of a PPy/C hybrid phase. Based on these results, our developed flash heat treatment successfully achieved partial carbonization of the organic shell in the core-shell silicon-based composite, constructing a functional hybrid-phase medium layer of highly conductive carbon/highly flexible PPy on the silicon surface. This medium layer synergizes the high conductivity and rigidity of carbon with the inherent elasticity of the PPy polymer network, thereby enhancing electrical conductivity while maintaining structural stability and exhibiting superior adaptability to silicon volume expansion. Consequently, the modified nmSi@PCHS-5 demonstrated significantly improved cycling stability compared to nmSi@C and nmSi@PPy, proving the superiority of this inorganic carbon/organic hybrid phase as a coating layer for silicon-based anodes.

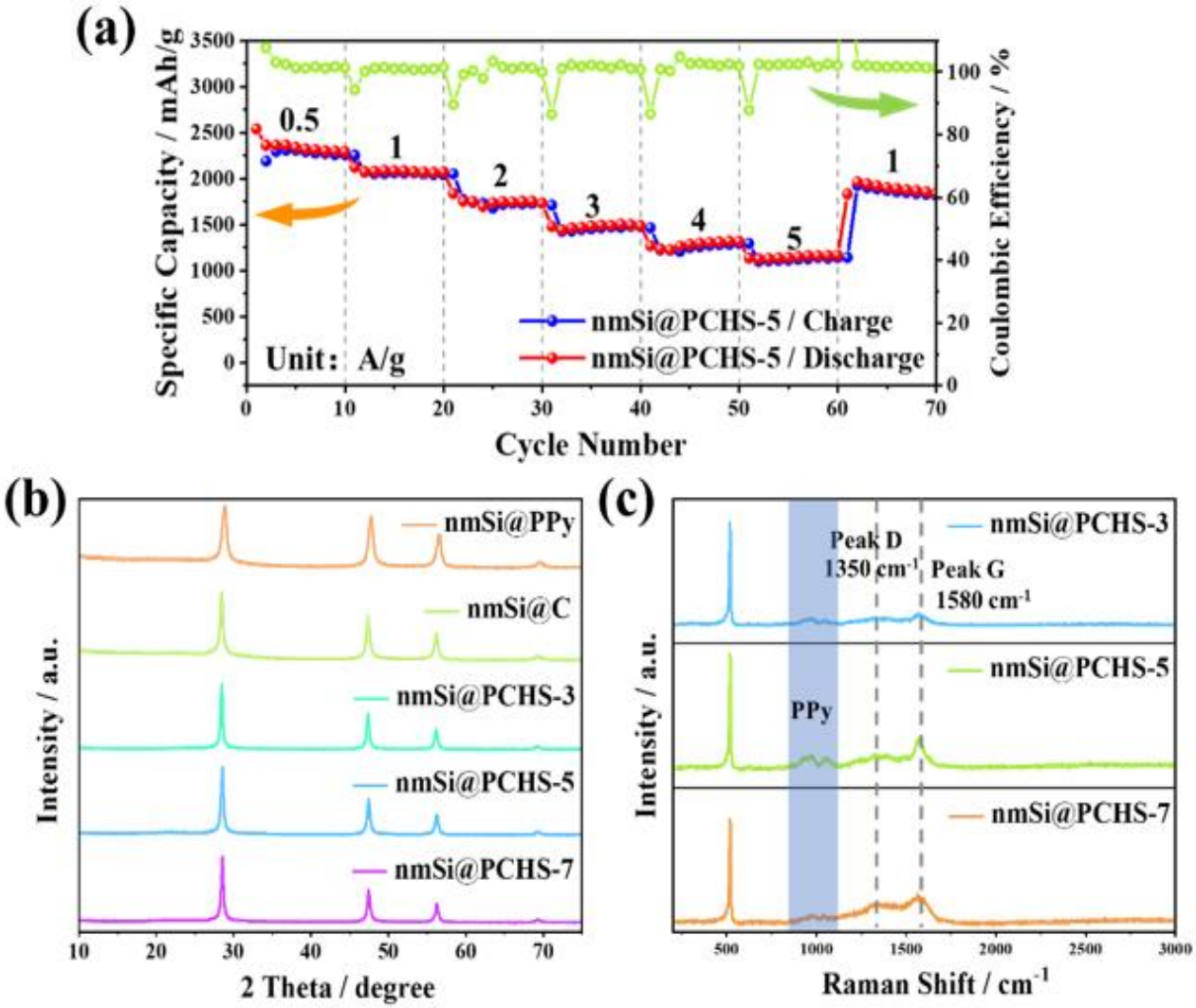

Fig 3. (a) Step discharge/charge behavior with varying current density of nmSi@PCHS-5. (b) XRD spectra of nmSi@PPy, nmSi@C, nmSi@PCHS-3, nmSi@PCHS-5 and nmSi@PCHS-7. (c) Raman spectra of nmSi@PCHS-3, nmSi@PCHS-5 and nmSi@PCHS-7.

Subsequently, the nmSi@PCHS-5 material demonstrating optimal performance was selected for further characterization to analyze its performance enhancement mechanism. First, the Si content in the composite material was determined via thermogravimetric analysis (TG). According to TG results, the composite exhibited a weight loss rate of approximately 30% when calcined in air, indicating a silicon loading of about 70% (Fig. 4a). Raman spectroscopy confirmed the successful preparation of the composite through characteristic peaks corresponding to Si, PPy, and C (Fig. 4b). Microstructural characterization revealed a core-shell configuration in nmSi@PCHS-5, where the PPy/C hybrid shell uniformly encapsulated the Si core. The spherical particles exhibited a diameter of approximately 260 nm, resembling small particle clusters with uniform size and excellent dispersion, facilitating homogeneous distribution in electrode slurries (Fig. 4c). Elemental mapping demonstrated uniform distribution of Si, C, and O throughout the sample. Carbon primarily originated from the PPy/C hybrid layer, while oxygen derived from oxygen-containing functional groups in the shell and the silicon surface oxide layer (Fig. 4d and e). The uniform and dense surface coating buffered volume changes in the silicon core while isolating electrolyte contact, promoting stable solid electrolyte interphase formation.

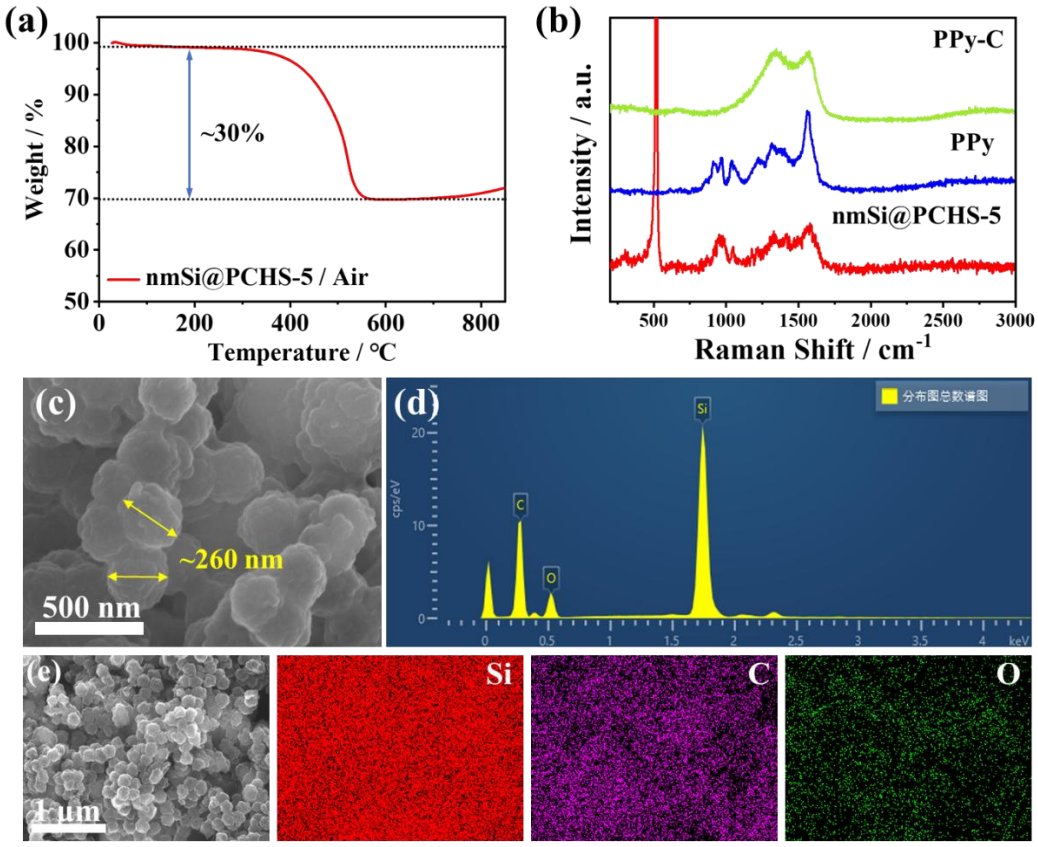

Fig 4. (a) TGA curves of nmSi@PCHS-5 in air. (b) Raman spectra of PPy-C, PPy and nmSi@PCHS-5. (c) SEM iamge of nmSi@PCHS-5. (d) elemental analysis of nmSi@PCHS-5 obtained by energy dispersive spectroscopy (EDS). (e) SEM and elemental mapping images of nmSi@PCHS-5.

Electrochemical impedance spectroscopy of nmSi@PCHS-5 and pure nmSi electrodes revealed lower resistance for nmSi@PCHS-5 both initially and after 100 cycles (Fig. 5a and b). This confirmed that the PPy/C hybrid layer enhanced electrical conductivity and facilitated conductive network formation within the electrode. Furthermore, cyclic voltammetry (CV) curves at various scan rates and pseudocapacitance contribution fitting results demonstrated superior lithiation/delithiation kinetics in nmSi@PCHS-5 (Fig. 5c-f). The contributions from diffusion-controlled and pseudocapacitive-controlled processes in the electrode were quantified using the following equation (Eqs. (1), (2)):

$$i=k_1v+k_2v^{1/2} \quad (1)$$

$$i/v^{1/2}=k_1v^{1/2}+k_2 \quad (2)$$

Here k_1v and $k_2v^{1/2}$ represent the pseudocapacitive and diffusion contributions, respectively. The figure illustrates the variation of capacitive contributions with scan rates for both nmSi@PCHS-5 and pure nmSi electrodes. As the scan rate increases from 0.1 mV/s to 0.5 mV/s, the proportion of capacitive contributions gradually rises. Notably, compared to nmSi, the nmSi@PCHS-5 electrode exhibits a larger pseudocapacitive contribution across all scan rates. It has been demonstrated that the non-diffusion-controlled component favors electrochemical behavior at high rates.[17] Therefore, nmSi@PCHS-5 demonstrates superior electrochemical stability and ion conductivity. Correspondingly, the lower pseudocapacitive contribution of nmSi at high scan rates indicates its limited electrochemical activity under high-rate conditions. Finally, the surface morphologies of nmSi@PCHS-5 and pure nmSi electrodes after cycling were observed via SEM (Fig. 5g-l). Significant cracks appeared on the nmSi electrode surface after 50 cycles, which propagated after 100

cycles, eventually forming spider-web-like through-thickness cracks (Fig. 5g-i). This structural damage led to loss of electrical contact, active material detachment, continuous formation of new SEI, and electrolyte decomposition, ultimately causing rapid capacity decay, increased internal resistance, and other severe issues. In contrast, nmSi@PCHS-5 exhibited a more stable electrode structure. After 50 and 100 cycles, the surface compactness increased, with only minor cracks observed that did not further develop into a spider-web pattern (Fig. 5j-l). This phenomenon directly confirms the superior effectiveness of the PPy/C hybrid layer as a flexible buffer layer: The inherent elasticity and toughness of PPy, combined with the mechanical strength and conductivity of the carbon material, synergistically absorb and dissipate the substantial stress generated by volume changes in the Si core during lithiation/delithiation, significantly reducing stress concentration. Simultaneously, the coating layer acts as a physical barrier, reducing direct contact between silicon active material and the electrolyte, thereby suppressing the continuous formation of unstable SEI films on freshly exposed crack surfaces. Lastly, the PPy/C hybrid layer provides excellent conductivity. Even when minor cracks occur, the hybrid layer's inherent conductive network and its good interfacial contact with silicon particles are maintained, ensuring that efficient charge transport pathways are not extensively severed. Consequently, this stable structural design drives comprehensive improvement in electrochemical performance, significantly enhances the cycling stability of silicon anodes, and provides crucial technical support for the practical application of high-energy-density Si-based anodes.

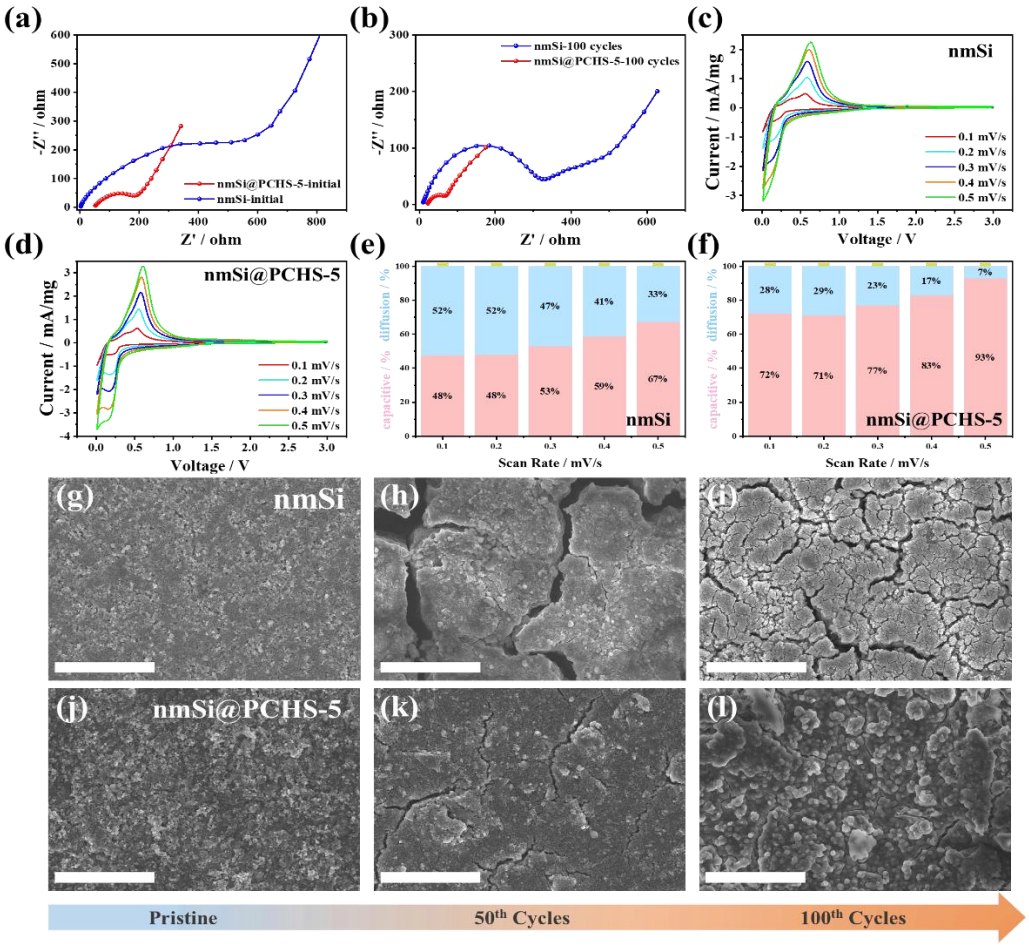

Fig 5. The Nyquist plots of nmSi and nmSi@PCHS-5 at (a) initial state and (b) 100 cycles. CV curves at different scan rates from 0.1 to 0.5 mV/s of (c) nmSi and (d) nmSi@PCHS-5. Capacitive and diffusion-controlled contributions to the total capacity at scan rates from 0.1 to 0.5 mV/s of (e) nmSi and (f) nmSi@PCHS-5 electrodes. SEM images of (g-i) nmSi and (j-l) nmSi@PCHS electrodes (surface) in different cycles.

4. Conclusions

In summary, this study successfully developed a novel flash heat treatment strategy for preparing high-performance Si anode materials. By subjecting polypyrrole (PPy)-coated Si nanoparticles (nmSi) to rapid high-temperature processing, we achieved partial carbonization of the organic coating, resulting in nmSi@PCHS composites featuring a unique organic polymer/inorganic carbon (PPy/C) hybrid shell. Systematic characterization (XRD, Raman spectroscopy, SEM, TG) confirmed the composite's core-shell structure and composition. The duration of heat treatment was identified as a critical parameter, with an optimal window around 5 minutes. The resulting nmSi@PCHS-5 balances sufficient carbonization for enhanced conductivity while retaining adequate flexible polypyrrole to accommodate volume changes. Electrochemical evaluation demonstrated that nmSi@PCHS-5 exhibits exceptional cycling stability (1000 mAh/g after 500 cycles at 1 A/g) and rate capability (1200 mAh/g at 5 A/g). Post-cycling SEM analysis revealed only minor cracks in nmSi@PCHS-5 electrodes, contrasting with severe fracturing in nmSi electrodes. This work highlights the effectiveness of flash heat treatment for creating multifunctional hybrid interfacial layers on silicon nanoparticles. The resulting PPy/C hybrid shell synergistically combines the high conductivity and mechanical strength of carbon with the inherent elasticity and toughness of polypyrrole. This simultaneously addresses silicon anodes' critical challenges—poor conductivity and significant volume expansion—providing important insights for practical applications of silicon-based anodes in next-generation high-energy-density lithium-ion batteries.

Acknowledgements

This work was supported by the Young Taishan Scholars Program of Shandong Province (tsqn202211082), Natural Science Foundation of Shandong Province (ZR2023MB051, ZR2024QE082), National Natural Science Foundation of China (52277229, 52202337, 22371153), National Key Research and Development of China (2022YFA1503402), and the Fundamental Research Funds for the Central Universities (22CX06023A, 24CX07003A, 2462023QNXZ015, 25CX07005A).

References

[1] Yu Z, Rudnicki P E, Zhang Z, et al. Rational solvent molecule tuning for high-performance lithium metal battery electrolytes[J]. Nature Energy, 2022, 7(1): 94-106.

[2] Xue W, Huang M, Li Y, et al. Ultra-high-voltage Ni-rich layered cathodes in practical Li metal batteries enabled by a sulfonamide-based electrolyte[J]. Nature Energy, 2021, 6(5): 495-505.

[3] Choi J W, Aurbach D. Promise and reality of post-lithium-ion batteries with high energy densities[J]. Nature Reviews Materials, 2016, 1(4): 16013.

[4] Rahman M A, Song G, Bhatt A I, et al. Nanostructured Silicon Anodes for High-Performance Lithium-Ion Batteries[J]. Advanced Functional Materials, 2015, 26(5): 647-678.

[5] Yu R, Pan Y, Jiang Y, et al. Regulating Lithium Transfer Pathway to Avoid Capacity Fading of Nano Si Through Sub-Nano Scale Interfused SiOx/C Coating[J]. Advanced Materials, 2023, 35(49).

[6] He Y, Jiang L, Chen T, et al. Progressive growth of the solid–electrolyte interphase towards the Si anode interior causes capacity fading[J]. Nature Nanotechnology, 2021, 16(10): 1113-1120.

[7] Liu D, Cao G. Engineering nanostructured electrodes and fabrication of film electrodes for efficient lithium-ion intercalation[J]. Energy & Environmental Science, 2010, 3(9).

[8] Tan D H S, Chen Y-T, Yang H, et al. Carbon-free high-loading silicon anodes enabled by sulfide solid electrolytes[J]. Science, 2021, 373(6562): 1494-1499.

[9] Wang F, Chen G, Zhang N, et al. Engineering of carbon and other protective coating layers for stabilizing silicon anode materials[J]. Carbon Energy, 2019, 1(2): 219-245.

[10] Li H, Wan Z, Wu T, et al. Modified polyacrylonitrile cross-linked with carboxymethyl cellulose constructing a hydrogen bonding network for high-performance silicon anodes[J]. Inorganic Chemistry Frontiers, 2023, 10(23): 7073-7081.

[11] Wang W, Wang Y, Huang W, et al. In Situ Developed Si@Polymethyl Methacrylate Capsule as a Li-Ion Battery Anode with High-Rate and Long Cycle-Life[J]. ACS Applied Materials & Interfaces, 2021, 13(5): 6919-6929.

[12] Schnabel M, Harvey S P, Arca E, et al. Surface SiO2 Thickness Controls Uniform-to-Localized Transition in Lithiation of Silicon Anodes for Lithium-Ion Batteries[J]. ACS Applied Materials & Interfaces, 2020, 12(24): 27017-27028.

[13] Li N, Yi Z, Lin N, et al. An Al2O3 coating layer on mesoporous Si nanospheres for stable solid electrolyte interphase and high-rate capacity for lithium-ion batteries[J]. Nanoscale, 2019, 11(36): 16781-16787.

[14] Ma Q, Xie H, Qu J, et al. Tailoring the Polymer-Derived Carbon Encapsulated Silicon Nanoparticles for High-Performance Lithium-Ion Battery Anodes[J]. ACS Applied Energy Materials, 2019, 3(1): 268-278.

[15] Luo W, Chen X, Xia Y, et al. Surface and Interface Engineering of Silicon-Based Anode Materials for Lithium-Ion Batteries[J]. Advanced Energy Materials, 2017, 7(24).

[16] Li L, Du B, Yang Y, et al. Ionic/Electronic Dual-Conductor Coating Layer Fabrication Enabling High-Performance Silicon Anode[J]. Small Structures, 2022, 4(2).

[17] Liu S, Liu B, Yu Z, et al. Rapid Release of Silicon by Ultrafast Joule Heating Generates Mechanically Stable Shell–Shell Si/C Anodes with Dominant Inward Deformation[J]. ACS Nano, 2024, 18(26): 17326-17338.